State-Feedback Control of Ball-Plate System: Geometric Approach

Khalid Lefrouni, Saoudi Taibi
Mohammed V University in Rabat, Rabat, Morocco

***Abstract*—This research focuses on investigating the issue of accurately controlling the location of the ball in the ball and plate system. The findings of this research have practical applications across several domains, including optimizing the alignment of solar panels to enhance their energy generation capacity. In this work, we propose the development of a system dynamics model using the Euler-Lagrangian approach. Furthermore, we analyze a technique in the frequency domain known as the geometric approach to create a state-feedback control that ensures the stability of the system. This study primarily focuses on analyzing the characteristic equations associated with the closed-loop system, while also considering the impact of feedback delay. Ultimately, the proposed technique is substantiated by presenting simulation data for validation.**

***Keywords*—Ball-plate system; Delay systems; Geometric approach; State-feedback control**

I. INTRODUCTION

We are intrigued by this article's exploration of the issue of position control of the ball in the ball and plate system. The main objective is to accurately identify the stable region of the closed-loop system. The parameters within this region ensure system stability. Consequently, additional requirements can be incorporated into the controller, with the aim of finding the optimal parameters within this region that not only guarantee stability, but also achieve a desired level of precision and speed for the system.

This objective is achieved by utilizing both state feedback control and a frequency analysis technique known as the Geometric method [2]. To evaluate the efficiency of the developed controllers, we have opted to focus on a highly responsive technology known as the Ball and Plate technology. The potential uses of this research are manifold, such as utilizing sensors to assess radiation and then adjusting the panel support to optimize the orientation of solar panels and enhance their efficiency.

Multiple control rules have been devised to regulate the location of the ball on the plate [1]-[4]-[7]-[8]. Nevertheless, the majority of these studies rely on a real-time model [5], which entails a continuous measurement in real-time. However, this hypothesis fails to accurately capture the actual dynamics of the system [3].

The ball and plate structure is a development of the ball and beam system. Due to its uncomplicated setup and easy implementation, it has become a much sought-after device for controller implementation. By utilizing the touch screen as a position sensor in conjunction with a standard PID controller, it is possible to conduct real-world experiments [13]-[14]. Furthermore, a ball and plate system was created for educational purposes [15]-[16]. Several academics have developed a fuzzy control method using this teaching equipment [17]-[18].

Due to the more advanced study on the ball-beam systems, we were particularly interested in the models referenced in sources [6]-[9]. These models may be classified into two distinct types. The first group employs neutral functional differential equations [11], whereas the second category utilizes retarded functional differential equations [9]-[12].

Therefore, we suggest utilizing a ball and plate system model that relies on retarded functional equations [9], together with frequency domain synthesis techniques (refer to [2] and [10]), to construct a state feedback control rule [2]. This method may ascertain the stability zone of the system in the control parameter space, while considering the impact of feedback delay. Consequently, it is permissible to choose the parameters of the control rule that fall inside the stable zone and satisfy the necessary specifications.

The subsequent sections of this article are structured in the following manner. Section 2 presents the ball and plate system model, which is based on retarded functional equations. In Section 3, we focus on the synthesis of state feedback control laws to guarantee the stability of the closed-loop system. Section 4 presents an illustrative scenario taken from existing literature, and simulations validate the suggested methodology. Ultimately, we arrive to a conclusion in Section 5.

NOMENCLATURE

L_X	Plate length in x-direction
L_Y	Plate length in y-direction
r_M	Motor arm length
r_b	Ball radius
m_b	Ball mass
J_b	Moment of inertia of the ball
α	Plate angle around the x-axis
β	Plate angle around the y-axis
ϑ_x	Motor angle around the x-axis
ϑ_y	Motor angle around the y-axis
K	State feedback gain
$x(t)$	State space vector
τ_x	System feedback delay along the x-axis
τ_y	System feedback delay along the y-axis
Ω	Set of crossing frequency

II. BALL AND PLATE SYSTEM MODELING

In this section we will determine the linear model of the ball and Plate system (see Fig. 1). For this, we will first apply Lagrange's method, then we will linearize the model found around the operating point. Finally we will present the model in the state space.

A. Preliminaries

Considering E_k and E_p respectively the kinetic and potential energy of the system.

The Lagrangian equation is then expressed as:

$$\frac{\partial}{\partial t}\left(\frac{\partial L}{\partial \dot{x}}\right) - \frac{\partial L}{\partial x} = 0 \quad (1)$$

with

$$L = E_k - E_p \quad (2)$$

The total kinetic energy of the ball is equal to the sum of the translational kinetic energy $E_{k,T}$ and the rotational kinetic energy $E_{k,R}$ with:

$$E_{k,T} = \frac{1}{2} m_b v_b^2 = \frac{1}{2} m_b (\dot{x}_b^2 + \dot{y}_b^2) \quad (3)$$

$$E_{k,R} = \frac{1}{2} J_b \omega_b^2 = \frac{1}{2} J_b \frac{(\dot{x}_b^2 + \dot{y}_b^2)}{r_b^2} \quad (4)$$

Thus

$$E_k = \frac{1}{2}\left(m_b + \frac{J_b}{r_b^2}\right)(\dot{x}_b^2 + \dot{y}_b^2) \quad (5)$$

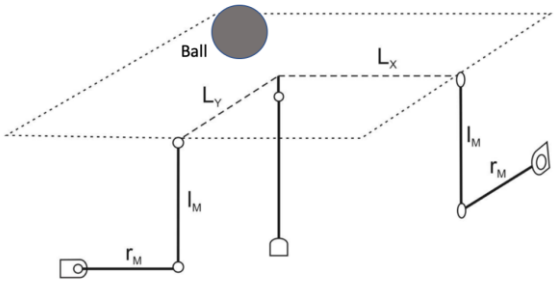

Fig. 1. Structure of the ball and plate system.

Taking into consideration the angles between the plate and the axes Ox and Oy (see Fig. 2), the potential energy can be expressed by:

$$E_p = -m_b g x_b \sin(\alpha) - m_b g y_b \sin(\beta) \quad (6)$$

Thus

$$L = \frac{1}{2}\left(m_b + \frac{J_b}{r_b^2}\right)(\dot{x}_b^2 + \dot{y}_b^2) + m_b g x_b \sin(\alpha) + m_b g y_b \sin(\beta) \quad (7)$$

So applying the Lagrangian Eq. (1) where L is described by Eq. (7), we have:

$$\frac{\partial}{\partial t}\left(\frac{\partial L}{\partial \dot{x}}\right) = \frac{\partial}{\partial t}\left(\left(m_b + \frac{J_b}{r_b^2}\right)\dot{x}_b\right) = \left(m_b + \frac{J_b}{r_b^2}\right)\ddot{x}_b \quad (8)$$

$$\frac{\partial L}{\partial x} = m_b g \sin(\alpha) \quad (9)$$

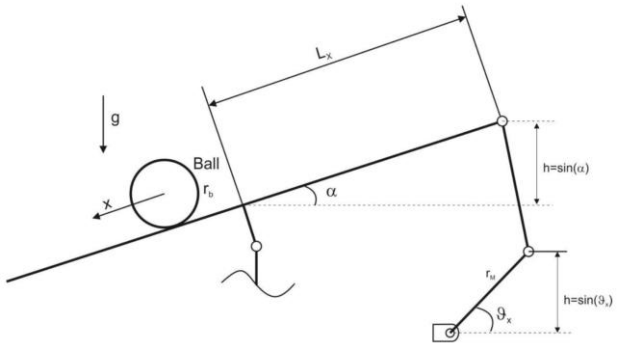

Fig. 2. Side view of the ball and plate system.

After simplification, we therefore have the differential equation of the motion of the ball along the x-axis :

$$\ddot{x}_b = \frac{m_b g r_b^2}{m_b r_b^2 + J_b} \sin(\alpha) \quad (10)$$

Similarly, following the same steps, the differential equation of the motion of the ball along the y-axis is described by the following equation.

$$\ddot{y}_b = \frac{m_b g r_b^2}{m_b r_b^2 + J_b} \sin(\beta) \quad (11)$$

In order to determine a mathematical model between the inputs of the system (ϑ_x and ϑ_y) and the outputs of the system (x, y).

From Fig. 2 we can write :

$$\sin(\vartheta_x)\, r_M = sin(\alpha) L_X = h \quad (12)$$

By combining (10) and (12), we have:

$$\ddot{x}_b = \frac{m_b g r_b^2\, r_M}{(m_b r_b^2 + J_b)\, L_X} \sin(\vartheta_x) \quad (13)$$

$$\ddot{y}_b = \frac{m_b g r_b^2\, r_M}{(m_b r_b^2 + J_b)\, L_Y} \sin(\vartheta_y) \quad (14)$$

B. The Linearized Model of the Ball-Plate System

The linearization of the model in Eq. (13), (14) around the operating point $(x = 0, y = 0)$, assuming a small variation of the ϑ_x and ϑ_y angles, leads us to the following equations :

$$\ddot{x}_b = G_x\, \vartheta_x \quad (15)$$

$$\ddot{y}_b = G_y\, \vartheta_y \quad (16)$$

with

$$G_x = \frac{m_b g r_b^2\, r_M}{(m_b r_b^2 + J_b)\, L_X} \quad \text{and} \quad G_y = \frac{m_b g r_b^2\, r_M}{(m_b r_b^2 + J_b)\, L_Y}$$

Remark :

Given the similarity of the x- and y-axis models, in the following we will start the study based on the x-axis modeling and deduce at the end the results for the y-axis.

As a result, the state space model of the Ball and Plate System along the x-axis can be written as follows:

$$\begin{cases} \dot{x}(t) = A\,x(t) + B\,u(t-\tau_x) \\ y(t) = C\,x(t) \end{cases} \quad (17)$$

Where $x(t) = [x_b(t) \quad \dot{x}_b(t)]^T$ is the state vector, $u(t) = \vartheta_x(t)$ is the input, τ_x is the feedback delay and

$$A = \begin{bmatrix} 0 & 1 \\ 0 & 0 \end{bmatrix}, \qquad B = \begin{bmatrix} 0 \\ G_x \end{bmatrix}, \qquad C = [1 \quad 0]$$

III. State-Feedback Controller

This part will concentrate on the construction of a state feedback controller in order to guarantee the stability of the closed-loop system. As stated previously, we will employ a geometric approach [2] to identify the specific area in the control parameter space where stability may be guaranteed.

A. Geometric Approach Principle

The geometric technique [2] is a frequency-based methodology that enables the determination of stability areas and regions where the measurement error converges to zero during the synthesis of the observer. Hereafter, we just provide the fundamental aspects to resolve this issue.

B. Stability Regions

Next, we will implement the various stages of the geometric technique to determine the stability region of the closed-loop system.

The state feedback controller is characterized by:

$$u(t) = -K_x\,x(t) \quad (18)$$

K_x is the state feedback gain that guarantees the stability of the system (17) for any $\tau_x < \tau_x^*$ (where τ_x^* is the maximum delay τ_x).

If the controllability of (A, B) is assumed, the goal is to find the gain K_x that will define the characteristic equation of the closed-loop system:

$$H(s, e^{-\tau_x s}) = \det(sI_2 - (A - BK_x\,e^{-\tau_x s}))=0 \quad (19)$$

is Hurwitz for any $\tau_x < \tau_x^*$

By employing the Laplace transform, we can express the system as follows:

$$\begin{cases} s\,x(s) = A\,x(s) + B\,u(s)e^{-\tau_x s} \\ y(s) = C\,x(s) \end{cases} \quad (20)$$

Also, the state-feedback controller takes the following form:

$$u(s) = -K_x\,x(s) \quad (21)$$

where, $K_x = [k_{x1} \quad k_{x2}]$ is the state feedback gain.

The characteristic equations related to the closed-loop system are as follows:

$$H(s, k_{x1}, k_{x2}, \tau_x) = Q(s) + P(s)e^{-\tau_x s} \quad (22)$$

The polynomials $Q(s)$ and $P(s)$ are defined as follows:

$$Q(s) = s^2, \quad P(s) = G_x(sk_{x2} + k_{x1}) \quad (23)$$

The characteristic Eq. (22) has real coefficients, therefore, the conjugate of each root is also a solution of this equation, so we have the following equations:

$$\begin{aligned} H(s, k_{x1}, k_{x2}, \tau_x) &= Q(s) + P(s)e^{-\tau_x s} = 0 \\ H(-s, k_{x1}, k_{x2}, \tau_x) &= Q(-s) + P(-s)e^{\tau_x s} = 0 \end{aligned} \quad (24)$$

In this analysis, we will start by examining a zero-delay closed-loop system and endeavor to identify conditions that govern the corrector parameters and guarantee the system's stability (17).

$H(s, k_{x1}, k_{x2}, 0) = 0$ is thus the Hurwitz characteristic polynomial. More precisely, for the complex left half-plane to contain all of its roots, the following conditions must be met:

$$k_{x1} > 0, \; k_{x2} > 0 \quad (25)$$

This represents a first requirement on the parameters of the controller.

C. Crossing Curves

For determining the gain K_x that guarantees the roots are distributed in the complex left half plane, one must initially identify the parameters of the state feedback gain K_x that contain a minimum of one pure imaginary root in the characteristic equation (19). This is the same as attempting to solve the equation:

$$\forall \omega > 0, \; \tau_x^* \in \mathcal{R}^+, \; H\left(j\omega, e^{-j\omega\,\tau_x^*}\right) = 0 \quad (26)$$

The retrieved K-parameters define the so-called crossing points. Consequently, this enables the generation of crossing curves in the region of the parameters (k_{x2}, k_{x1}).

By considering the system (17), we can define the crossing points in the space (k_{x2}, k_{x1}) as follows:

Proposition 1

For a delay $\tau_x^* > 0$ and $\omega \in \Omega$, the crossing points are defined by the following equations:

$$k_{x1} = \frac{\omega^2 \cos(\omega\tau_x^*)}{G_x} \quad (27)$$

$$k_{x2} = \frac{\omega\, sin(\omega\tau_x^*)}{G_x} \quad (28)$$

where Ω is the set of frequencies and $\omega \in \mathcal{R}^+$ such that $H(j\omega, k_{x1}, k_{x2}, \tau_x^*) = 0$ has at least one solution (k_{x1}, k_{x2}).

Proof: From the characteristic equation (26) we have :

$$-\omega^2 + G_x(j\omega k_{x2} + k_{x1})e^{-j\omega\,\tau_x^*} = 0$$

Then, considering the real and imaginary parts, we get :

$$\begin{cases} -\omega^2 + G_x(\omega k_{x2}\sin(\omega\,\tau_x^*) + k_{x1}\cos(\omega\,\tau_x^*)) = 0 \\ \omega k_{x2}\cos(\omega\,\tau_x^*) - k_{x1}\sin(\omega\,\tau_x^*) = 0 \end{cases}$$

Solving these two equations leads to Eq. (27) and (28).

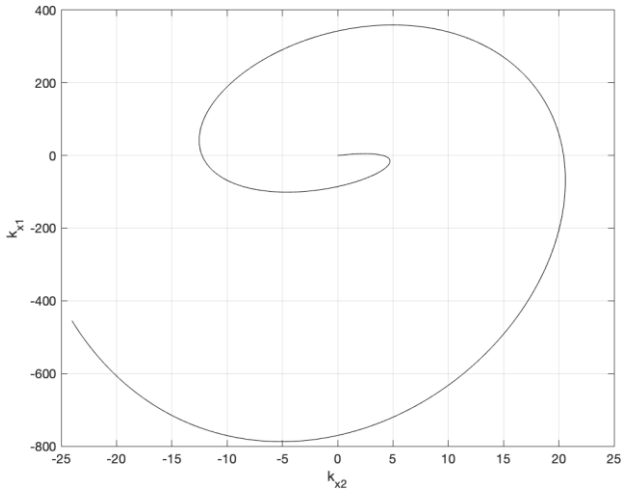

Fig. 3. Crossing curves with $\tau_x^* = 0.3$.

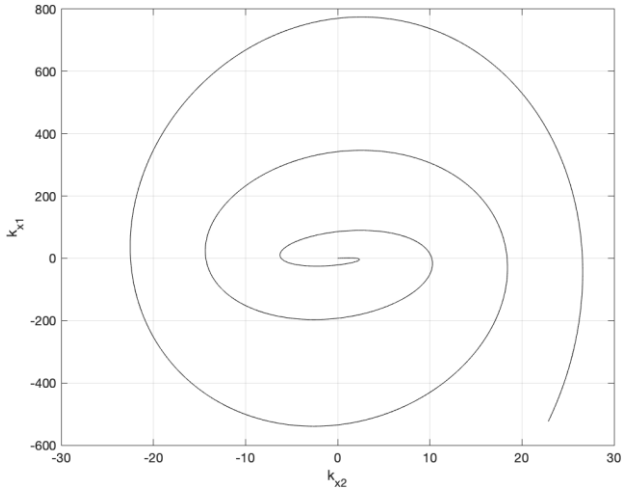

Fig. 4. Crossing curves with $\tau_x^* = 0.6$.

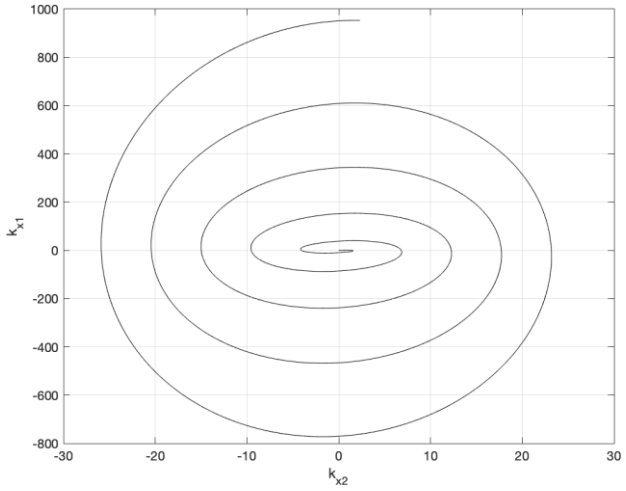

Fig. 5. Crossing curves with $\tau_x^* = 0.9$.

Therefore, through the examination of various delay values $\tau_x^* \in \{0.3, 0.6, 0.9\}$, the crossing curves illustrated in Fig. 3, Fig. 4 and Fig. 5. The provided curves illustrate the progression of the controller parameters (k_{x2}, k_{x1}) in response to variations in the system's pulsation which the Eq. (27) and (28) describe.

D. Direction of the Crossing

Using the approach detailed in [2], we can determine the direction of the crossing. To do so, we have to consider the numbers R_i and I_i, defined by:

$$\begin{aligned} R_0 + jI_0 &= j\frac{\partial H(s,k_{x1},k_{x2},\tau_x^*)}{\partial s}\Big|_{s=j\omega} \\ R_1 + jI_1 &= -\frac{1}{s}\frac{\partial H(s,k_{x1},k_{x2},\tau_x^*)}{\partial k_{x2}}\Big|_{s=j\omega} \\ R_2 + jI_2 &= -\frac{1}{s}\frac{\partial H(s,k_{x1},k_{x2},\tau_x^*)}{\partial k_{x1}}\Big|_{s=j\omega} \end{aligned} \quad (29)$$

By applying the principles outlined in reference [2], it is now possible to ascertain the direction of crossing, which denotes the path followed by the roots of $H(j\omega, k_{x1}, k_{x2}, \tau_x^*) = 0$ as they traverse the imaginary axis.

Mathematically, a direction going from left to right is translated by the following inequality:

$$R_2 I_1 - R_1 I_2 > 0$$

Thus, taking into consideration the expression of the numbers R_i and I_i defined by (29), after calculation we have :

$$R_2 I_1 - R_1 I_2 = \frac{{G_x}^2}{\omega} > 0 \quad (30)$$

We can therefore deduce that the direction of the crossing is to the right.

E. Regions of Stability

Using the findings from the preceding sections, we will now identify the areas of stability for the system. This implies that all values of the gains K_x, for which the Eq. (19) is Hurwitz for any delay τ_x belongs to the interval $[0, \tau_x^*]$.

Thus, taking into consideration condition (25) on the one hand, and the crossing curve that delimits the stability region on the other hand, we have identified the stability region of the closed-loop system. Fig. 6 illustrates this region in case $\tau_x^* = 0.6\ s$.

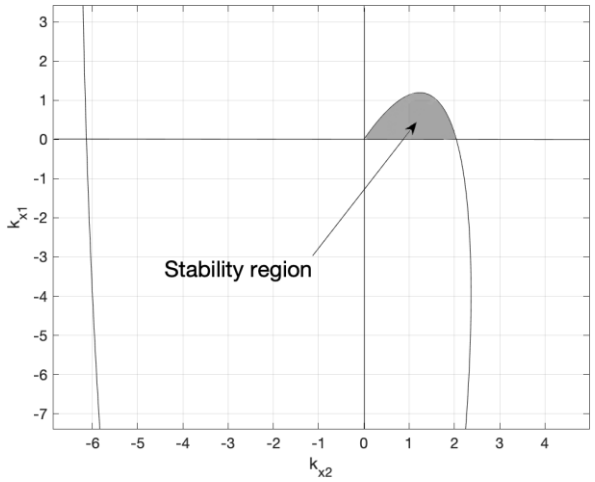

Fig. 6. The stability area of a closed loop system with $\tau_x^* = 0.6$

Every set of parameters $(k_{x1}^*,\ k_{x2}^*)$ inside the shown region in Fig. 6, determines a gain $K_x^* = [k_{x1}^*\ \ k_{x2}^*]$ which guarantees the closed-loop system's stability for any delay τ_x such that $\tau_x < \tau_x^*$. Subsequently, we will determine the critical delay value τ_x^* , beyond which stability cannot be assured.

Proposition 3. Critical delay

The state feedback controller $u(t) = -K_x^*\, x(t)$, with $K_x^* = [k_{x1}^*\ \ k_{x2}^*]$, asymptotically stabilizes the closed loop system (17) for any $\tau_x < \tau_x^*$, such as τ_x^* is defined by:

$$\tau_x^* = \frac{1}{\omega}\, Arccos\left[\frac{k_{x1}^*\,\omega^2}{G_x\left((k_{x1}^*)^2+(\omega k_{x2}^*)^2\right)}\right] \tag{31}$$

Proof: Considering the characteristic Eq. (22) and positioning at the limit of stability, i.e., assuming that it admits a root $s = j\omega$, we thus have:

$$Q(j\omega) + P(j\omega)e^{-j\omega\tau_x^*} = 0 \tag{32}$$

Using the expression of P and Q and the formula of Euler, we thus have:

$$\cos(\omega\,\tau_x^*) - \mathrm{j}\,\sin(\omega\,\tau_x^*) = \frac{k_{x1}^*\,\omega^2 - j\omega^3\,k_{x2}^*}{G_x((k_{x1}^*)^2 + (\omega k_{x2}^*)^2)}$$

By equality of the real parts of this equation we obtain the relation in Eq. (31)

Proposition 4. Critical frequency of crossing

The critical frequency of crossing ω_0 is defined by:

$$\omega_0 = \sqrt{\frac{\alpha_1+\sqrt{\alpha_1^2+4\alpha_0}}{2}} \tag{33}$$

With

$$\alpha_0 = (G_x k_{x1}^*)^2 \quad \text{and} \quad \alpha_1 = (G_x k_{x2}^*)^2$$

Proof: From Eq. (32), we have:

$$e^{-j\omega\tau_x^*} = \frac{-Q(j\omega)}{P(j\omega)} \tag{34}$$

$$e^{j\omega\tau_x^*} = \frac{-Q(-j\omega)}{P(-j\omega)} \tag{35}$$

By multiplying the two Eq. (34) and (35), we have:

$$Q(j\omega)Q(-j\omega) - P(j\omega)P(-j\omega) = 0$$

After simplification, we have the following equation:

$$\omega^4 - \alpha_1\omega^2 - \alpha_0 = 0 \tag{36}$$

By solving this equation and considering only positive frequencies, we find the result in Eq. (33).

F. Results for the y-axis

The state feedback controller providing closed-loop system stability along the y-axis is defined by:

$$u(t) = -K_y\, x(t) \tag{37}$$

where, $K_y = [k_{y1}\ \ k_{y2}]$ is the state feedback gain and $x(t) = [y_b(t)\ \ \dot{y}_b(t)]^T$ is the state vector.

Taking into consideration the expression of the numbers R_i and I_i, defined by Eq. (29), after calculation we have :

$$R_2I_1 - R_1I_2 = \frac{{G_y}^2}{\omega} > 0 \tag{38}$$

So we have the same results along the y-axis, i.e. a direction of passage from left to right.

Based on this result on the one hand and on the crossing curve that delimits the region of stability on the other hand, we have thus determined the region in which all the roots of the characteristic equation have a strictly negative real part, in other words, we have identified the region of stability of the closed-loop system that controls the evolution of the ball along the y-axis.

Therefore, Fig. 7 illustrates the stability region for $\tau_y^* = 0.8\ s$

Also, the critical delay is specified as:

$$\tau_y^* = \frac{1}{\omega}\, Arccos\left[\frac{k_{y1}^*\,\omega^2}{G_y\left((k_{y1}^*)^2+(\omega k_{y2}^*)^2\right)}\right] \tag{39}$$

Where the gain of state feedback $K_y^* = \left[k_{y1}^*\ \ k_{y2}^*\right]$ stabilizes the closed-loop system for any delay τ_y that is less than τ_y^* .

IV. Simulation

We will now illustrate the results found in the preceding sections. Thus, the ball and plate system described in Section 2 is taken into consideration, its dynamics are determined by Eq. (13) and (14) with: $L_X = 0.134\,m$, $L_Y = 0.168\,m$, $r_M = 0.0245\,m$, $r_b = 0.02\,m$, $J_b = 0.0000416\,kg*m^2$, $m_b = 0.26\,kg$. And the system feedback delay along the x-axis and the y-axis are respectively $\tau_x = 0.6s$, $\tau_y = 0.8s$.

Thus, considering the regions of stability shown in Fig. 6 and Fig. 7, we arbitrarily choose two pairs $(k_{x1}^*,\ k_{x2}^*) = (0.45,\ 0.6)$ and $(k_{y1}^*,\ k_{y2}^*) = (0.35\ ,\ 0.75)$.

i.e.

$$K_x = [0.45 \quad 0.6] \tag{40}$$

$$K_y = [0.35 \quad 0.75] \tag{41}$$

From Eq. (31) and (39), we then calculate the critical values of feedback delays:

$$\tau_x^* = 0.9403\ ,\ \tau_y^* = 1.2399 \tag{42}$$

Which means that the state feedback gains K_x and K_y stabilize the system (17) such that τ_x and τ_y both fall within the intervals $[0,\ 0.9403)$ and $[0,\ 1.2399)$, respectively.

We then get, on the one hand, Fig. 8 and Fig. 9, which illustrate the evolution over time of the ball position defined by the coordinates $(x_b\ , y_b)$, and on the other hand, Fig. 10 illustrates the evolution of the ball on the plate in the $(x\ , y)$ plane.

Now, choose two other pairs inside the stability regions illustrated in Fig. 6 and Fig. 7.

$$(k_{x1}^*,\ k_{x2}^*) = (0.25,\ 1.7) \quad (43)$$

$$(k_{y1}^*,\ k_{y2}^*) = (0.55\ ,\ 1.45) \quad (44)$$

Thus, we find the evolution of the ball coordinates $(x_b\ , y_b)$ presented in Fig. 11, Fig. 12, Fig. 13, and the critical values of the delays :

$$\tau_x^* = 0.6888\ ,\ \tau_y^* = 0.8694 \quad (45)$$

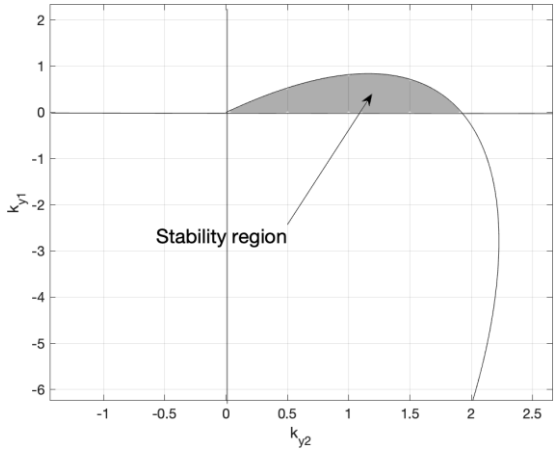

Fig. 7. The stability area of a closed loop system with $\tau_y^* = 0.8$.

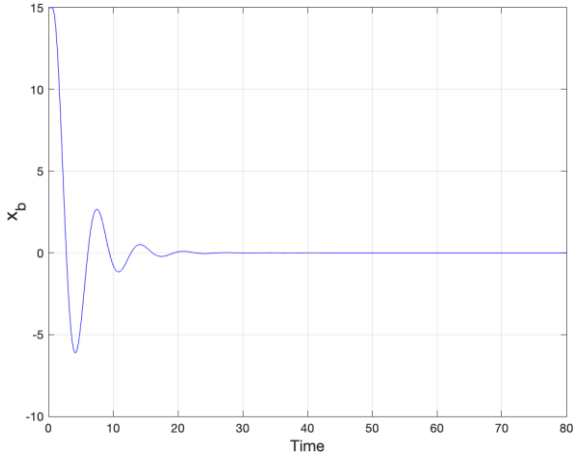

Fig. 8. Temporal evolution of x_b with the state feedback gain (40).

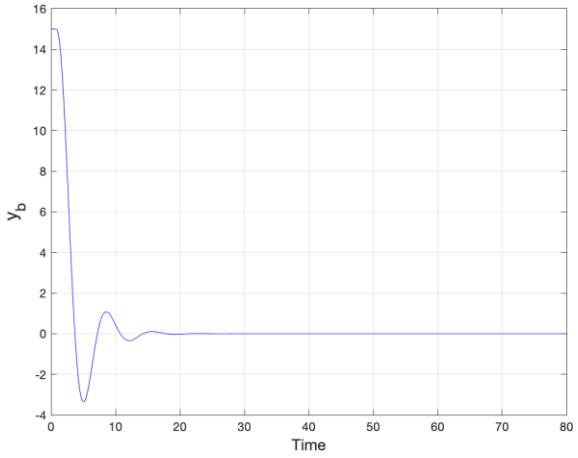

Fig. 9. Temporal evolution of y_b with the state feedback gain (41).

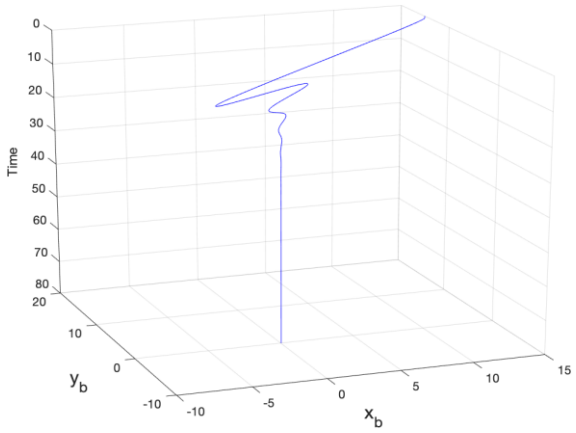

Fig. 10. Evolution of the position of the ball with the state feedback gains (40) and (41).

Comparing the results illustrated in Fig. 10 and Fig. 13, we can see that a slight change in the values of the gains K_x and K_y leads, on the one hand, to a decrease in the critical values of the delays τ_x and τ_y (See results (42) and (45)), and consequently to a restriction on the permitted values of the delays, and, on the other hand, to an increase in the oscillations, which leads to an increase in the system response time.

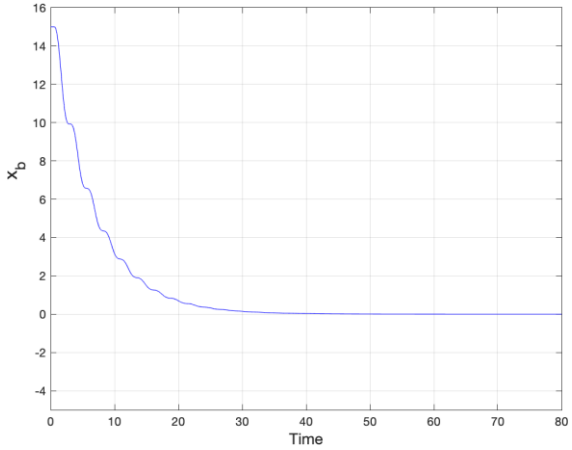

Fig. 11. Temporal evolution of y_b with the state feedback gain (43).

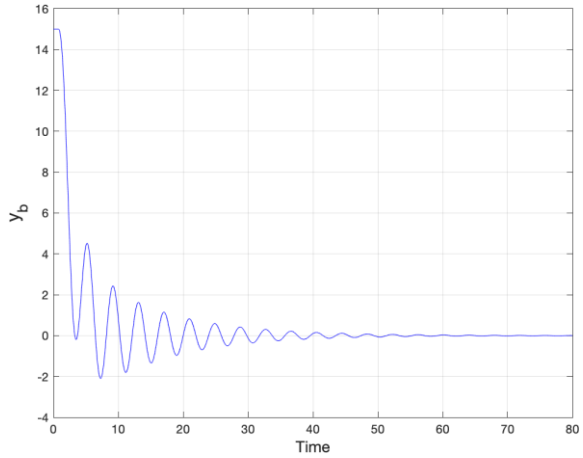

Fig. 12. Temporal evolution of y_b with the state feedback gain (44).

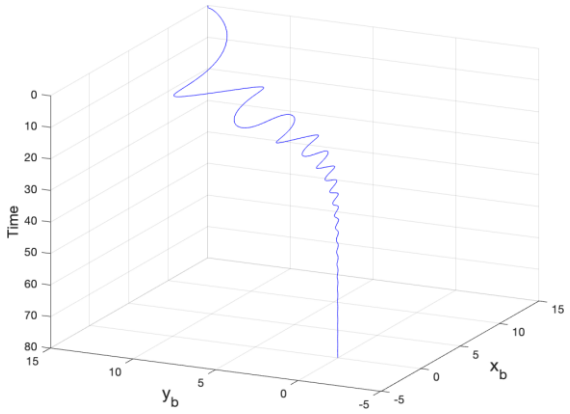

Fig. 13. Evolution of the position of the ball with the state feedback gains (43) and (44).

It therefore seems that it is imperative to develop an algorithm to identify the best gains belonging to the stability regions that best meet the required specifications.

V. CONCLUSION

This article examines the issue of control in the ball and plate system. By analyzing the impact of feedback delays and employing a geometric methodology, we have identified the range of gains that guarantee the system stability. Subsequently, we demonstrated the feasibility of this method using a simulated analysis. It should be mentioned, however, that to guarantee the validity of these results, an accurate measurement of the system's state is required. Thus, in future work, we will enhance the efficacy of the controller through the implementation of an observer such as the Luenberger observer. Also to improve the performance of the controller, we will prioritize the creation of an algorithm that enables the selection of suitable gains, considering the attributes of the transient regime, such as response time, rise time, and overshoot.

REFERENCES

[1] E.F. Sinaga, E.B. Manurung, V.A. Chee and A. Djajadi, "Building and controlling a ball and plate system," International Conference on Advances in Communication Network and Computing, March 2011.

[2] K. Lefrouni and R. Ellaia, "State-feedback control in TCP network: geometric approach," International Review of Automatic Control, vol. 8, pp. 127-133, 2015.

[3] F. Dušek, D. Honc and K. R. Sharma, "Modelling of ball and plate system based on first principle model and optimal control," 21st International Conference on Process Control, Strbske Pleso, pp. 216-221, 2017.

[4] B. Heeseung and L. Young, "Implementation of a ball and plate control system using sliding mode control," IEEE Access, pp. 32401-32408, vol. 10, May 2018.

[5] A. Knuplez, A. Chowdhury and R. Svecko, "Modeling and control design for the ball and plate system," pp. 1064-1067, vol. 2, 2004.

[6] B. Meenakshipriya, K. Kalpana, "Modelling and control of ball and beam system using coefficient diagram method (CDM) based PID controller," IFAC Proceedings Volumes, vol. 47, pp. 620-626, 2014.

[7] C.C. Ker, C. E. Lin and R. T. Wang, "Tracking and balance control of ball and plate system," Journal of the Chinese Institute of Engineers, vol. 30:3, pp. 459-470, 2007.

[8] D. Xiucheng, Z. Yunyuan, X. Yunyun, Z. Zhang and S. Peng, " Design of PSO fuzzy neural network control for ball and plate system," International Journal of Innovative Computing, Information and Control, vol. 7, pp. 7091-7103, 2011.

[9] G. Buza, T. Insperger, "Mathematical models for balancing tasks on a see-saw with reaction time delay," IFAC-Papers OnLine, vol. 51, pp. 288-293, 2018.

[10] W. Michiels and S. Niculescu, "Stability and stabilization of time-delay systems: an eigenvalue-based approach," Advances in Design and Control, 2007.

[11] H. Eduardo, H. Hernán and M. Mark, "Existence of solutions for second order partial neutral functional differential equations," Integral Equations and Operator Theory, vol. 62, pp. 191-217, 2008.

[12] T.H. Baker, "Retarded differential equations," Journal of Computational and Applied Mathematics, vol 125, pp. 309-335, 2000.

[13] J. H. Park and Y. J. Lee, "Robust visual servoing for motion control of the ball on a plate," Mechatronics, vol. 13, Iss. 7, pp. 723-738, September 2003.

[14] C. Cheng and C. Tsai, "Visual servo control for balancing a ball-plate system," International Journal of Mechanical Engineering and Robotics Research, vol. 5, no. 1, pp. 28-32, January 2016.

[15] A. Kastner, J. Inga, T. Blauth, F. Köpf, M. Flad and S. Hohmann, "Model-based control of a large-scale ball-on-plate system with experimental validation," IEEE International Conference on Mechatronics, 18-20 March 2019.

[16] C. Ionescu, E. Fabragas, S. Cristescu, S. Dormido and R. De Keyser, "A remote laboratory as an innovative educational tool for practicing control engineering concepts," IEEE Transactions on Education, 56(4), pp. 436-442, November 2013.

[17] R. Singh and B. Bhushan," Real-time control of ball balancer using neural integrated fuzzy controller," Artificial Intelligence Review, vol. 53, pp. 351–368, 2020.

[18] E. Zakeri, S.A. Moezi and M. Eghtesad, "Tracking control of ball on sphere system using tuned fuzzy sliding mode controller based on artificial bee colony algorithm," Int. J. Fuzzy Syst, vol. 20, pp. 295-308, 2018.